Journal of Testing and Evaluation

doi:10.1520/JTE20220236 / Vol. 51 / No. 4 / 2023 / available online at www.astm.org

Vitor S. Barbosa,[1] Vinicius M. C. Gomes,[1] and Claudio Ruggieri[2]

Temperature Dependence of Cleavage Fracture Toughness for an Ultrahigh Strength Martensitic Steel

Reference

V. S. Barbosa, V. M. C. Gomes, and C. Ruggieri, "Temperature Dependence of Cleavage Fracture Toughness for an Ultrahigh Strength Martensitic Steel," *Journal of Testing and Evaluation* 51, no. 4 (July/August 2023): 2598–2615. https://doi.org/10.1520/JTE20220236

ABSTRACT

This work conducts an exploratory evaluation of the brittle fracture behavior for an ultrahigh strength martensitic steel using conventional three-point bend SE(B) and precracked Charpy V-notch (PCVN) specimens. A primary purpose of this study is to verify the effectiveness of the Master Curve methodology in providing a reliable estimate of the reference temperature (T_0) derived from fracture toughness data sets measured in the ductile-to-brittle transition (DBT) region of an ultrahigh strength, low alloy martensitic steel. Fracture toughness testing conducted on three-point bend SE(B) specimens and PCVN configurations at different test temperatures in the DBT region provides the cleavage fracture resistance data in terms of the *J*-integral at cleavage instability, J_c, and its corresponding K_{Jc}-values for the tested material. Although this class of ultrahigh strength steel having a martensitic microstructure is currently beyond the reach of ASTM E1921, *Standard Test Method for Determination of Reference Temperature, T0, for Ferritic Steels in the Transition Range*, the analyses described here show that the predicted normalized curves of median fracture toughness versus temperature are in good agreement with the experimental measurements.

Keywords

master curve, reference temperature, fracture toughness, ductile-to-brittle transition temperature, ultrahigh strength martensitic steel

Manuscript received May 16, 2022; accepted for publication November 22, 2022; published online February 7, 2023. Issue published July 1, 2023.

[1] Department of Naval Architecture and Ocean Engineering, University of São Paulo, São Paulo 05508, Brazil

[2] Department of Naval Architecture and Ocean Engineering, University of São Paulo, São Paulo 05508, Brazil (Corresponding author), e-mail: claudio.ruggieri@usp.br, https://orcid.org/0000-0003-0600-3424

Introduction

Substantial progress has been made in recent years to characterize fracture behavior over the ductile-to-brittle transition (DBT) region and, more specifically, the dependence of fracture toughness data on temperature for ferritic steels. Early attention has been

primarily focused on improved integrity assessments of irradiated reactor pressure vessel (RPV) steels for the continued operation of nuclear power plants. Here, routine surveillance programs focused on the use of small fracture specimens, predominantly precracked Charpy V-notch (PCVN) specimens, to assess material degradation directly connected to changes in fracture toughness properties over the reactor operational life. However, the often insufficient capacity of small specimens to provide fracture toughness measurements under well-contained crack-tip plasticity for common pressure vessel and structural steels potentially lead to a marked increase, often associated with large statistical scatter, in measured values of cleavage fracture toughness (such as the *J*-integral at cleavage instability, J_c, or its equivalent elastic-plastic stress intensity factor, K_{Jc}). These features greatly complicate and add to the problem of correlating small specimen data with the fracture behavior of engineering structural components.

Wallin[1–3] advanced the viewpoint of a normalized curve describing the dependence of fracture toughness curve on temperature, as typified by the conventional ASME reference curves, to incorporate the effects of specimen size and statistical scatter on fracture toughness data over the DBT region. The procedure, known as the Master Curve (MC) approach,[1–5] defines an indexing (or reference) temperature, T_0, related to the median fracture toughness of K_{Jc}-values experimentally measured from standard 1T fracture specimens (with thickness $B = 25$ mm). Several previous studies[3,5,6] have shown that the MC methodology is highly effective in describing the dependence of fracture toughness on temperature for a wide range of structural ferritic steels, including irradiated conditions, with a yield strength in the range of 275∼825 MPa. The MC methodology has been standardized in the form of ASTM E1921 (ASTM E1921-21a, *Standard Test Method for Determination of Reference Temperature, T_0, for Ferritic Steels in the Transition Range*) and has also been incorporated into the ASME code.[7]

In view of the technological importance of assessing the fracture integrity of containment vessels, engineering applications of the MC procedure have been primarily focused on describing the temperature dependence of fracture toughness for pressure vessel steels and low-carbon structural steels. Moreover, the approach has also been shown to hold for tempered martensitic steels having very high strength, provided they can be considered as falling into the category of ferritic steels for which the MC method is applicable (ASTM E1921-21). Indeed, recent works of Odette et al.,[8,9] Neimitz et al.,[10,11] and Wallin et al.[12] provide support to use the MC approach in characterizing the fracture toughness transition behavior for this class of material. More specifically, Odette et al.[9] obtained good agreement between the fracture toughness transition curve defined by ASTM E1921-21a and the dependence of measured K_{Jc}-values on temperature for a structural martensitic steel employed in fusion reactors known as F82H steel.[13] In their work, they justify their findings by arguing that the MC transition temperature indexed by T_0 is mainly controlled by the statistically-based model to correct fracture toughness values for specimen thickness in connection with appropriate size requirements to prevent effect of constraint loss on measured K_{Jc}-values rather than details of the specific steel microstructure.

However, despite these advancements, more systematic studies to support the extension of the methodology to characterize the dependence of fracture toughness on temperature in ultrahigh strength steels (UHSS) with nominal strengths exceeding 1,000∼1,200 MPa remain limited. UHSS materials have been increasingly used in several engineering applications that require wear-resistant properties, such as excavator buckets and bulldozer blades, and in lightweight construction, especially for the structural members of mobile equipment, including chassis and superstructures for commercial vehicles, to reduce weight and fabrication costs. The application of such UHSS is rarely limited by inadequate strength but rather by other factors such as fracture properties. Although rather extensive experimental data exist for UHSS steels, the majority of data focuses on tensile and impact (Charpy V-notch) properties. Consequently, further extensions and applications of the MC methodology to describe the fracture toughness dependence of temperature for this class of material are largely justified as such studies can broaden the toughness-temperature relationship in the transition temperature for the existing toughness database of common structural steels to more advanced structural steels.

As a step in this direction, this work addresses an experimental investigation of the brittle fracture behavior for an ultrahigh strength martensitic steel using fracture toughness data measured in the ductile-to-brittle transition region (DBT). A primary purpose of this study is to assess the applicability of the MC methodology to

describe the fracture toughness transition curve indexed by the reference temperature T_0 for a direct-quenched, low alloy martensitic steel. Fracture toughness testing conducted on three-point bend SE(B) specimens and PCVN configurations at different test temperatures in the DBT region provides the cleavage fracture resistance data in terms of the *J*-integral at cleavage instability, J_c, and its corresponding K_{Jc}-values for the tested ultrahigh strength steel. Although this class of ultrahigh strength steel having a martensitic microstructure is currently beyond the reach of ASTM E1921-21a, the analyses described here show that the predicted normalized curves of median fracture toughness versus temperature are in good agreement with the experimental measurements.

Overview of the MC Approach

This section describes essential characteristics and steps of the data analysis method to determine the reference temperature, T_0, from experimentally measured fracture toughness values. Only salient features of the MC methodology are described here. Readers are referred to the works of McCabe et al.,[5] IAEA TR429,[14] ASTM E1921-21a, and references therein for details. The presentation that follows addresses both the single temperature method and the multi-temperature procedure.

SINGLE TEMPERATURE MC METHOD

The fundamental importance of assessing the integrity of RPVs (and other types of pressure vessels in general) has motivated the early introduction of a fracture mechanics approach to ensure adequate safety margins against brittle fracture in service conditions incorporating a reference temperature index correlated with the material fracture toughness. The approach relies on a lower bound description of the variation of elastic fracture toughness values, K_{Ic}, with temperature in the form

$$K_{Ic} = A + B\exp(CT_R) \tag{1}$$

where *A*, *B*, and *C* are material constants and $T_R = T - T_{NDTT}$ is the reference temperature index normalized in terms of the nill ductility transition temperature, T_{NDTT},[15,16] often obtained by the drop weight test.[17] The normalization temperature, T_{NDTT}, is adopted as a means to incorporate the heat-to-heat differences in fracture toughness transition temperature of the tested material database, thereby collapsing the fracture toughness data onto a single curve. The above equation (1) is the basis of the reference toughness curves implemented into the ASME code.[7]

Wallin[1–3] advanced the concept of the ASME K_{Ic} reference curve to develop a more accurate and, at the same time, more effective procedure to characterize elastic-plastic fracture toughness data over the DBT region. The methodology led to the notion of a "master" fracture toughness transition curve and relies on the construction of a normalized curve of median fracture toughness values, defined in terms of the elastic-plastic stress intensity factor, K_{Jc}, rather than J_c, for high constraint fracture specimens having size of 1T ($B = 25$ mm) geometries with temperature. The approach begins by considering a three-parameter Weibull distribution[18,19] to characterize the distribution of elastic-plastic K_{Jc}-values in the form.[18]

$$F(K_{Jc}) = 1 - \exp\left[-\left(\frac{K_{Jc} - K_{\min}}{K_0 - K_{\min}}\right)\right]^{\alpha} \tag{2}$$

which is a three-parameter Weibull distribution[19] defined by the Weibull modulus, α, the scale parameter or characteristic toughness, K_0, and the threshold fracture toughness, $K_{\min}$ (observe that $F(K_{Jc}) = 0$ for $K_{Jc} \leq K_{\min}$). Following ASTM E1921-21a, parameter α takes the value of 4 under conditions pertaining to small scale yielding (SSY) near the crack tip and $K_{\min}$ is conveniently assigned a value of 20 MPa$\sqrt{\text{m}}$. Moreover, the elastic-plastic K_{Jc}-values are obtained directly from experimentally measured J_c-values using the standard relationship:

$$K_{Jc} = \sqrt{\frac{EJ_c}{(1-\nu^2)}} \tag{3}$$

where it is understood that plane-strain conditions are assumed with E representing the Young's modulus and ν the Poisson's ratio, which is usually taken as the standard value of 0.3. To insure SSY conditions at fracture, K_{Jc}-values exceeding the measuring capacity of the specimen defined by $K_{Jc-\max} = \sqrt{Eb_0\sigma_{ys}/M(1-\nu^2)}$, where b_0 denotes the original crack ligament size and the deformation limit, $M = b_0\sigma_{ys}/J$, is conservatively assigned a value of 30, are treated as censored data[19]—the above equation (2) thus becomes a right-censored Weibull distribution.[20]

Another important feature of adopting the statistical description of K_{Jc}-values expressed by equation (2) is that it advantageously allows the use of a simple weakest link statistics to correct measured toughness values for effects of thickness in the case of fracture tests performed on other than 1T specimens as

$$K_{Jc-1T} = 20 + (K_{Jc-X} - 20)\left(\frac{B_X}{B_{1T}}\right)^{1/4} \text{MPa}\sqrt{\text{m}} \tag{4}$$

where B_{1T} is the 1T specimen size (thickness of $B = 25$ mm) and B_X is the corresponding thickness of the test specimens. The above relationship implies that when the thickness of the test specimen is reduced by half, for example, to a $1/2T$ ($B = 12.5$ mm) geometry, the median fracture toughness of measured K_{Jc}-values for 1T size specimens decreases by a factor of ≈0.87.

The scale parameter, K_0, corresponding to the 63.2 % cumulative failure probability, is commonly evaluated by a standard maximum likelihood (ML) estimation procedure[19] (ASTM E1921-21a) thus yielding

$$K_0 = \left[\sum_{k=1}^{N} \frac{(K_{Jc,k} - 20)^4}{r}\right]^{1/4} + 20\,\text{MPa}\sqrt{\text{m}} \tag{5}$$

where N denotes the total number of tested specimens and r represents the number of valid tests (uncensored data). Limiting attention here to the case of cleavage fracture without any significant amount of ductile tearing, $r = N - c$, where c is the number of censored toughness data points, which are represented by the toughness values exceeding $K_{Jc-\max}$. Once K_0 is determined, the median toughness of the experimental data set, including, if any, the censored toughness values at the test temperature, is given by

$$K_{Jc-med} = 0.9124(K_0 - 20) + 20\,\text{MPa}\sqrt{\text{m}}. \tag{6}$$

The resulting fracture toughness transition curve for the material in terms of the median toughness, K_{Jc-med}, and the reference (indexing) temperature, T_0, for 1T specimens takes the form

$$K_{Jc-med} = 30 + 70\exp[0.019(T - T_0)]^{\circ}\text{C},\ \text{MPa}\sqrt{\text{m}} \tag{7}$$

where T is the test temperature. Although the above T_0-based MC has a similar appearance as the ASME K_{Ic} reference curve given by previous equation (1), it actually differs significantly in character as it incorporates a statistical size effect and provides a means to determine statistical tolerance bounds on fracture toughness data. Indeed, ASTM E1921-21a test standard also gives procedures to construct tolerance bounds for varying confidence levels of equation (7).

MULTI-TEMPERATURE MC METHOD

While the MC methodology was originally developed to characterize the fracture toughness transition curve based on a single set of toughness values measured at a single (fixed) temperature, the approach can be generalized to

treat multiple data sets obtained from fracture tests performed at different temperatures within the DBT region. This may be justified when, for example, testing small fracture specimens, particularly PCVN geometries, to obtain fracture toughness data in the case of limitations on material availability. Here, as the maximum measuring capacity of these specimens is approached, the number of measured K_{Jc}-values exceeding $K_{Jc-\max}$ at a given test temperature may become undesirably large, thereby compromising the practicality of the test procedure and, perhaps more importantly, accurate evaluations of T_0. To circumvent this potential difficulty, a multi-temperature method[4,5,21] (ASTM E1921-21a) can also be used to evaluate the reference temperature, T_0.

By assuming that a similar expression to equation (1) holds in the case of the temperature dependence of K_0 in the form

$$K_0 = A + B\exp[C(T - T_0)]^{\circ}\text{C},\ \text{MPa}\sqrt{\text{m}} \tag{8}$$

Wallin[21] obtained the ML estimate of T_0 for a randomly censored data set corresponding to different test temperatures as

$$\sum_{k=1}^{N}\frac{\delta_k \exp[C(T_k - T_0)]}{A - K_{\min} + B\exp[C(T_k - T_0)]} - \sum_{k=1}^{N}\frac{(K_{Jc,k} - K_{\min})^4 \exp[C(T_k - T_0)]}{\{(A - K_{\min}) + B\exp[C(T_k - T_0)]\}^5} = 0 \tag{9}$$

from which T_0 can be solved iteratively. In the above, the Kronecker delta, δ_k, is 0 for censored data or 1 for valid K_{Jc}-data. It may be noted that equation (7) is actually a special case of equation (9) when all K_{Jc}-values are derived from a single test temperature. Further observe that ASTM E1921-21a incorporates the above equation with $K_{\min} = 20\ \text{MPa}\sqrt{\text{m}}$ and $A = 31\ \text{MPa}\sqrt{\text{m}}$, $B = 77\ \text{MPa}\sqrt{\text{m}}$, and $C = 0.019^{\circ}\text{C}^{-1}$. The section titled "Multi-Temperature Method" addresses application of the multi-temperature method defined by equation (9) to the tested ultrahigh strength steel.

Experimental Procedures

MATERIAL DESCRIPTION AND MECHANICAL PROPERTIES

The material utilized in the fracture tests described next is a high-strength martensitic steel supplied by Usiminas Steel in Brazil as a hot rolled plate with thickness of 31.5 mm. This steel is designated as USI AR450 and has similar characteristics as a Hardox 450 steel. It is produced by hot rolling through a Continuous On-Line Control accelerated cooling process, similar to a Thermo-Mechanical Control Process, followed by direct quenching. **Table 1** lists the chemical composition for the tested material, which contains low carbon content to improve the plate weldability. The required mechanical strength and hardenability are then obtained by small additions of key microalloying elements, such as boron, chromium, niobium, vanadium, and titanium, as shown in **Table 1**. Metallographic examination of an etched surface of the tested steel (Nital 2 % for 20 s) displayed in **figure 1*A*** and **1*B*** revealed a predominantly lath martensite microstructure formed by long and thin plates in a side-by-side, parallel arrangement, as typically observed in steel alloys having a carbon content of less than approximately 0.60 wt. %.[22]

Mechanical tensile tests at room temperature (20°C) were conducted in accordance with ASTM E8/8M (ASTM E8/E8M-21, *Standard Test Methods for Tension Testing of Metallic Materials*) on standard tensile specimens 12.5 mm in diameter and extracted from the transverse plate direction at mid-thickness in the as-received

TABLE 1

Chemical composition of tested martensitic steel (% weight) measured by atomic emission spectroscopy (AES) according to ASTM E415-21, *Standard Test Method for Analysis of Carbon and Low-Alloy Steel by Spark Atomic Emission Spectrometry*. The content of iron is given by Fe balance

C	Mn	Cr	V	Nb	Ti	B	Ni	Si	Cu	P	S
0.22	1.38	0.24	0.003	0.029	0.035	0.001	0.02	0.34	0.01	0.016	0.003

FIG. 1 Microstructure for the tested high-strength martensitic steel (Nital 2 %). Etching time: 20 s (*A*) magnification: 200 *x*; (*B*) magnification: 500 *x*.

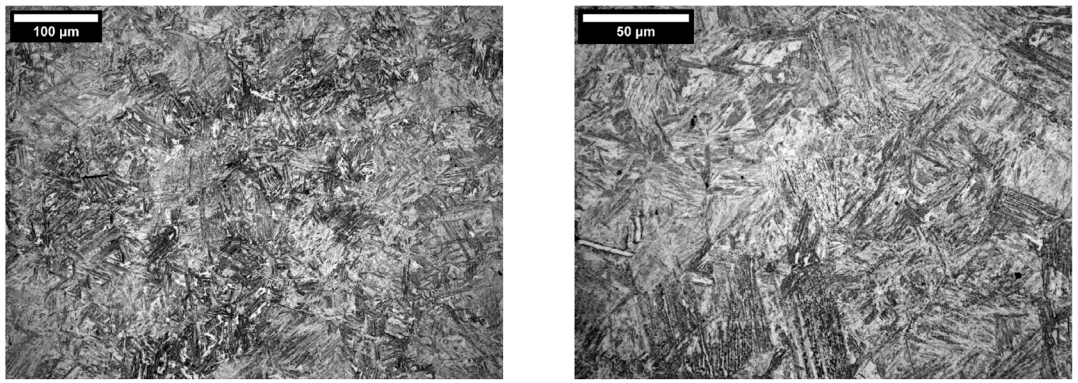

condition. The tensile properties of the tested steel (average of three tensile specimens) are defined by the yield stress, $\sigma_{ys} = 1{,}229$ MPa, and tensile strength, $\sigma_{uts} = 1{,}271$ MPa. **Figure 2*A*** provides the average engineering stress-strain response for the tested material, which clearly evidences the very low hardening behavior of this high-strength martensitic steel, as also indicated by a low σ_{uts}/σ_{ys}—ratio of 1.1. For completeness, an estimate of the Ramberg-Osgood exponent, n, to describe the power law approximation of the true stress-true strain behavior given by API 579[23] yields $n = 40$. Further, observe that the measured average value of yield stress far exceeds the upper limit of the yield stress range ($\sigma_{ys} \leq 825$ MPa) allowable by the MC approach.

Because the fracture tests are conducted at different DBT region temperatures (see further details next), the dependence of yield stress on temperature can be simply described by ASTM E1921-21a as

$$\sigma_{ys}^{T-test} = \sigma_{ys}^{RT} + \frac{10^5}{491 + 1.8T} - 189°\text{C, MPa}, \tag{10}$$

where σ_{ys}^{T-test} and σ_{ys}^{RT} define the material yield stress at the test temperature and at room temperature, respectively, and T is the test temperature. Similarly, the dependence of Young's modulus on temperature also follows from ASTM E1921-21a as

FIG. 2 Mechanical properties for the tested high-strength martensitic steel: (*A*) engineering stress- strain curves measured at room temperature and (*B*) Charpy-V impact energy (T-L orientation) versus temperature.

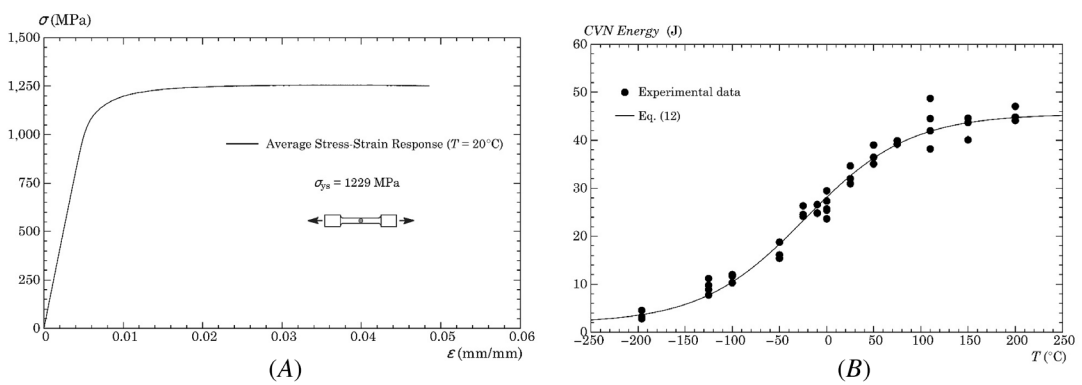

$$E = 204 - \frac{T}{16}\,^{\circ}\text{C, GPa.} \tag{11}$$

The above expressions and their corresponding estimates for the yield stress and Young's modulus define the specimen measuring capacity, as characterized by $K_{Jc-\max}$, at test temperature, which is required to perform the statistical analysis of the measured J_c-values and their correspondent K_{Jc}-values (refer to **Tables 2** and **3** in the "Temperature Effects on Fracture Toughness" section).

A set of standard Charpy V-notch (CVN) impact specimens was extracted from the mid-thickness of the plate in the T-L orientation and tested at different temperatures in a 406 J full-scale Tinius-Olsen pendulum machine following the requirements of ASTM E23 standard (ASTM E23-18, *Standard Test Method for Notched Bar Impact Testing of Metallic Materials*). **Figure 2B** shows the measured toughness-temperature properties in terms of conventional CVN impact energy in the T-L orientation. Here, because of the well-known dependence of fracture toughness on the rolling direction, the T-L orientation is chosen for the purpose of this investigation as it generally provides lower fracture toughness values compared to the T-L orientation. The symbols on the plot define the experimental values of Charpy energy, whereas the solid line describes a hyperbolic tangent curve fitting[24,25] in the form

$$CVE = 24 + 22\tanh\left[\frac{T+23}{110}\right]^{\circ}\text{C, J} \tag{12}$$

in which the lower shelf Charpy energy is taken as a constant value of 2 J, *CVE* denotes the Charpy V-notch energy, and T is the test temperature. Using the above expression, the Charpy transition temperatures corresponding to 28 J and 41 J energy yield approximately $T_{28J} = -2.8^{\circ}\text{C}$ and $T_{41J} = 90^{\circ}\text{C}$, respectively.

FRACTURE TOUGHNESS TESTING

To investigate the effects of temperature on the cleavage fracture behavior of the martensitic steel employed in this study, a series of fracture toughness tests was performed at different temperatures in the range of −20°C~70°C to measure the values of the *J*-integral at instability point, here defined as J_c, as shown previously in **figure 2B** - this temperature range falls within the middle to upper transition region for the tested steel. The fracture testing was conducted on three-point single edge- notched specimens, commonly designated as SE(B) configurations, also in the T-L orientation extracted from the mid-thickness of the plate. The SE(B) specimens have conventional,

TABLE 2

Measured fracture toughness values at the instability point, described in terms of J_c and corresponding K_{Jc}-values, for the high-strength martensitic steel obtained from standard 3P SE(B) specimens at $T = -20$°C, −10°C, 0°C, and 20°C

Specimen Configuration	T, °C	J_c, kJ/m²	K_{Jc}, MPa$\sqrt{\text{m}}$	a_0, mm	$M = (b_0\sigma_{ys}/J_c)$
1T SE(B)	−20	11	50	25.0	2,951
		18	64	25.4	1,588
		14	56	25.3	2,099
1T SE(B)	−10	30	82	25.0	1,073
		12	52	25.0	2,665
		16	59	25.5	2,011
1T SE(B)	0	15	57	25.2	2,184
		20	67	25.1	1,616
		17	62	25.7	1,830
1T SE(B)	20	33	86	25.5	943
		18	64	25.1	1,723
		25	74	25.7	1,253

TABLE 3

Measured fracture toughness values at the instability point, described in terms of J_c and corresponding K_{Jc}-values, for the high-strength martensitic steel obtained from standard 3P SE(B) specimens and the PCVN configuration at $T = 50°C$, 60°C, and 70°C

Specimen Configuration	T, °C	J_c, kJ/m²	K_{Jc}, MPa$\sqrt{m}$	a_0, mm	$M = (b_0\sigma_{ys}/J_c)$
1T SE(B)	50	43	97	24.9	737
		44	98	24.5	733
		45	100	25.2	682
		47	102	24.9	662
		53	108	25.6	582
		53	108	25.6	574
		56	111	25.5	548
		67	122	25.5	456
		85	137	25.0	369
1T SE(B)	60	76	129	25.3	408
		77	130	25.6	397
		78	131	25.3	395
		86	138	25.1	360
		90	140	25.0	348
		94	144	25.2	329
		94	144	25.2	327
		102	150	25.2	305
		110	155	24.9	285
1T SE(B)	70	95	144	25.6	320
		101	149	25.6	303
		101	149	25.5	301
		104	151	25.0	298
		105	152	25.7	286
		107	153	25.1	289
		110	155	25.6	276
		117	160	25.8	258
		139	175	25.5	218
PCVN	50	51	106	5.0	119
		56	111	5.4	100
		57	113	5.0	105
		62	117	5.3	92
		69	123	5.2	85
		102	150	5.3	56
		105	152	5.1	56
		106	153	5.3	54

plane-sided geometry with thickness, $B = 25.4$ mm (1T configuration), width $W = 50.8$ mm, loading span $S = 203.2$ mm, and a nominal crack length (a) to width (W) ratio of $a/W = 0.5$.

The fracture specimens were first fatigue precracked under a load ratio of $R = 0.1$ at approximately 20 Hz and then loaded under displacement control in three-point bending in an MTS Landmark servo-hydraulic testing machine in accordance with the test protocols specified in ASTM E1820 (ASTM E1820-21, *Standard Test Method for Measurement of Fracture Toughness*) and ASTM E1921-21a. For the fracture tests at low temperature ($-20°C \leq T \leq 0°C$), the SE(B) specimens were immersed in a nitrogen/alcohol bath and temperature controlled by two thermocouples (one at the specimen surface near the crack tip region and the other one immersed in the bath) wired to a digital thermometer. The thermocouples have a reading accuracy of ±1°C, thereby allowing a very good temperature control. For the fracture testing at higher temperature ($50°C \leq T \leq 70°C$), the SE(B) specimens

FIG. 3 Representative load-CMOD curves for the tested martensitic steel corresponding to different test temperatures: (*A*) $T = -20°C$, (*B*) $T = 20°C$, (*C*) $T = 50°C$, and (*D*) $T = 70°C$.

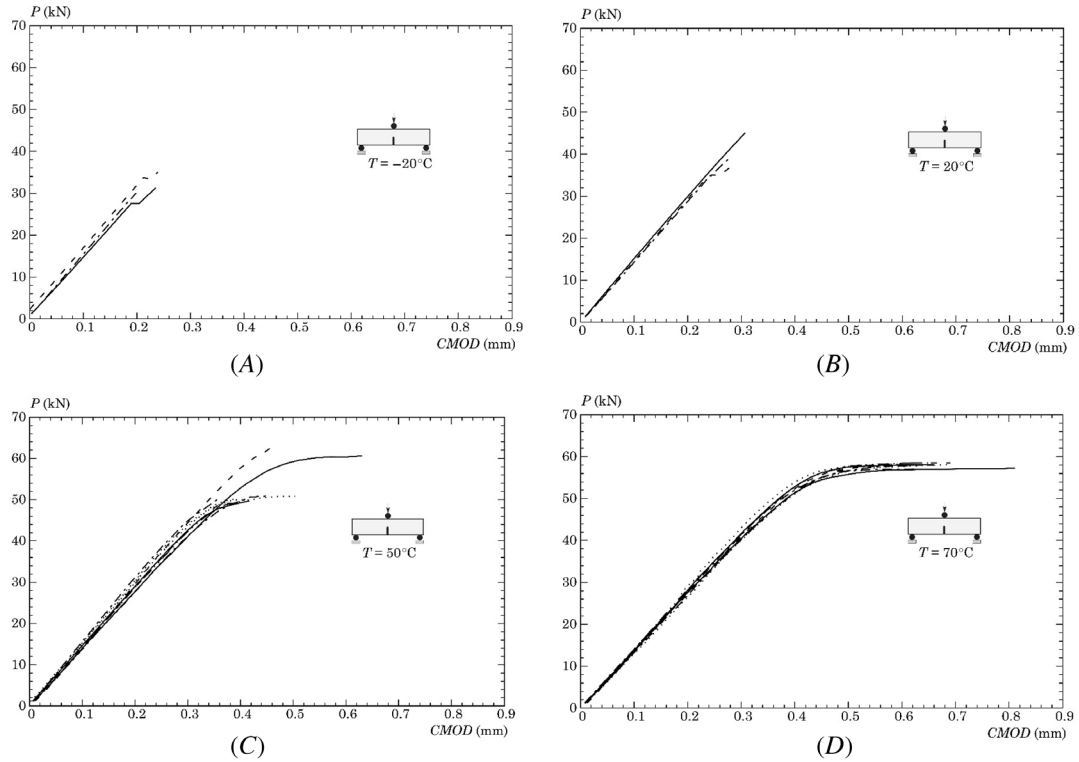

were immersed in a biodegradable soluble cutting oil/water bath with temperature also controlled by two thermocouples wired to a digital thermometer. For better temperature control, electric immersion heaters electrically operated by a contactor coupled to a thermostat circuit were used in the bath. Further, to avoid thermal gradients in the bath, a hot water recirculating pump was fixed inside the thermal box. Both cooling and heating bath temperature were then maintained during 20∼30 min at the specified test temperature before the test specimens were loaded. Records of load versus crack mouth opening displacement (CMOD) were measured in each specimen using a clip-on displacement gage mounted on an integrated knife-edge machined into the notch mouth. Post-test analysis of the fracture surfaces in conjunction with the nine-point measurement technique described in ASTM E1820-21 allowed the measurement of the initial crack size (a_o) and the amount of stable crack growth, if any, prior to final cleavage fracture in the tested specimens.

An important first step in applying the MC procedure involves the selection of an adequate test temperature from which the measured fracture toughness values can be used to determine T_0. Following ASTM E1921-21a, a convenient estimate of the indexing temperature, $\widetilde{T}_0$, for ferritic steels is given by $\widetilde{T}_0 = T_{28J} - 18°C$ or $\widetilde{T}_0 = T_{41J} - 24°C$, which yields $\widetilde{T}_{0-28J} = -20.8°C$ and $\widetilde{T}_{0-41J} = 66°C$ for the martensitic steel under consideration. If we tentatively accept the $\widetilde{T}_{0-28J}$ estimate as being close to correct, then we can set $T = -20°C$ as the initial test temperature. **Figure 3*A*** shows the load versus CMOD data for three specimens tested at $T = -20°C$, which reveals an essentially linear elastic brittle behavior with no plastic work under the load-displacement curve. Because the MC procedure requires elastic-plastic behavior, it is thus necessary to increase the test temperature, such as the fracture tests were performed at the temperatures $T = -20°C$, $-10°C$, $0°C$, $20°C$, $50°C$, $60°C$, and $70°C$. **Figure 3*B*–*D*** displays the load-displacement curves at three different test temperatures: $T = 20°C$, $50°C$, and

70°C. Consider first the load-CMOD results shown in figure 3*B*. Despite the increase in test temperature from −20°C to 20°C, an essentially linear elastic behavior still prevails, making this data set apparently not useful for the effective application of the MC approach. For completeness, Table 2 shows the fracture toughness at cleavage instability at $T = -20$°C, −10°C, 0°C, and 20°C, and also includes the average precrack fatigue length based on the nine-point measurement technique given by ASTM E1820-21 and the deformation limit, M, for each measured toughness data. Observe that this table displays only three fracture toughness values because it became clear at the start of the fracture tests at those test temperatures that the measured J_c-values would characterize essentially linear elastic behavior. Consider next the load-displacement records at $T = 50$°C and 70°C shown in figure 3*C* and 3*D*, respectively. A different picture now emerges as there is a relatively large fraction of the total area under the load-displacement curve associated to plastic work and, thus, to the plastic contribution to the strain energy for the crack configuration. With those factors taken into account, only the fracture toughness measured at $T = 50$°C, 60°C, and 70°C will be used in the present study.

To provide further experimental evidence of the well-contained plastic deformation at the crack tip for the selected measured fracture toughness data, figures 4 and 5 show typical macroviews of fracture surfaces and scanning electron microscopy examined very close to the crack-tip region for representative specimens tested at $T = 50$°C and 70°C. Figures 4*A* and 5*A* reveal that there is a well-defined transition between the tip of the fatigue precrack and the beginning of the fracture surface with no evidence of plastic deformation at the crack front and, perhaps more importantly, no signs of any amount of ductile tearing preceding brittle fracture. Now direct attention to the fracture surfaces displayed in figures 4*B* and 5*B*. At $T = 50$°C, the fracture surface pictured in figure 4*B* shows clear indications of a quasi-cleavage pattern with smaller cleavage facets mixed with dimple regions, which is a mixed mechanism involving both cleavage and microvoid coalescence typical of high strength steels.[10,26] Here, the highly dissipative process of void nucleation and growth eventually gives way to the formation of a larger secondary microcrack by void coalescence seen in figure 4*B* prior to unstable propagation of the macroscopic crack. Next focus on the fracture surface displayed in figure 5*B*, in which the corresponding fractography shows a predominantly dimple pattern with large primary voids, typically nucleated by fracture or decohesion of second-phase particles and nonmetallic inclusions, connected by numerous secondary voids. Because the specific character of these nonmetallic inclusions, such as the ones within some of the large dimples in figure 5*B*, does not have a direct bearing on the approach pursued in the present study, we did not conduct a more in-depth investigation to assess the grade and classify those nonmetallic inclusions. What is more important

FIG. 4 Typical macroviews of fracture surfaces and scanning electron microscopy (SEM) fractography (accelerating voltage of 20 kV and spot size of 10 nm) of the (*A*) crack front (35x) and (*B*) fracture process zone (1,000x) of specimen tested at $T = 50$°C.

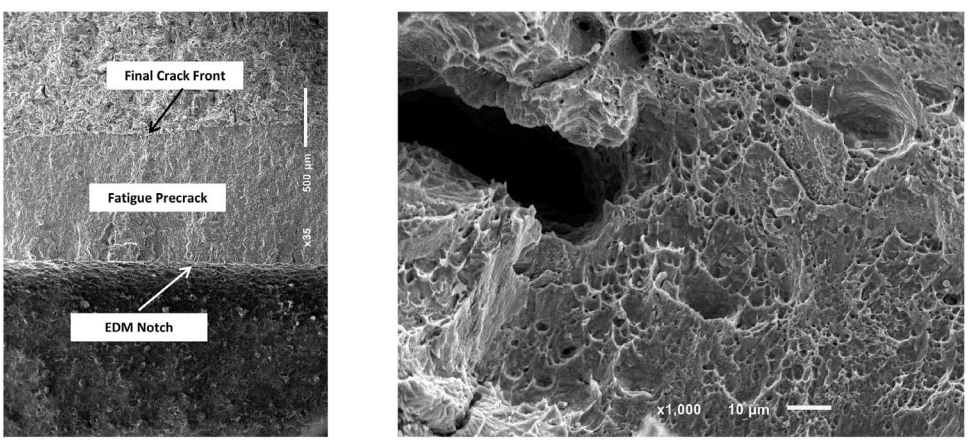

(*A*) (*B*)

FIG. 5 Typical macroviews of fracture surfaces and scanning electron microscopy (SEM) fractography (accelerating voltage of 20 kV and spot size of 10 nm) of the (*A*) crack front (35x) and (*B*) fracture process zone (1,000x) of specimen tested at $T = 70°C$.

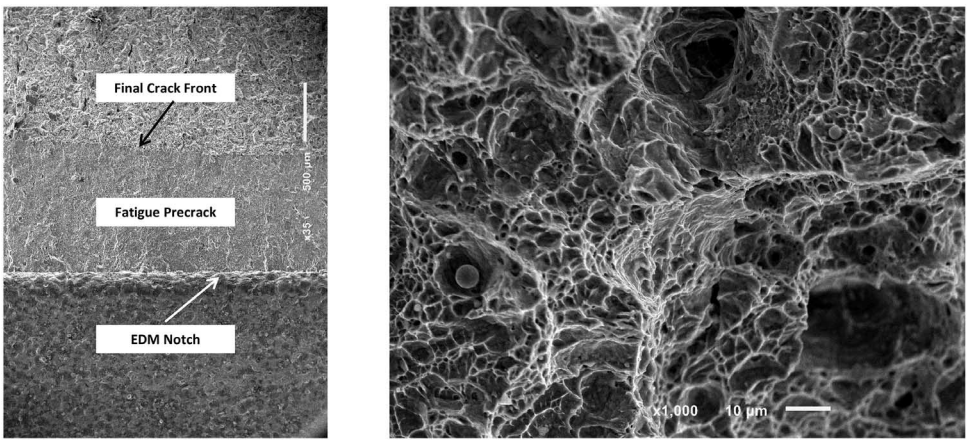

here, though, is that this is a surprising outcome because, as will be addressed later, the single temperature T_0 evaluated on the basis of the data set at $T = 70°C$ is in close agreement with the reference temperature at other test temperatures, which thus suggests that these dimple-related microscale processes do not affect the T_0-evaluation for this material. A discussion on the implications of this behavior on the MC procedure is postponed to the "Single-Temperature Method" section.

Figure 6 displays the cumulative probability distribution of the fracture toughness values in terms of K_{Jc}-values for the tested specimens at $T = 50°C$, 60°C, and 70°C. The plot also includes the measured K_{Jc}-values at $T = 50°C$ for the PCVN configuration. The solid symbols represent the experimental fracture toughness data for the specimens. Values of the cumulative failure probability, $F(K_{Jc})$, are obtained by ordering the K_{Jc}-values and using $F(K_{Jc}) = (k - 0.3)/(N + 0.4)$,[19] where k denotes the rank number and N defines the total number of

FIG. 6

Three-parameter Weibull distribution of experimentally measured K_{Jc}-values with varying test temperatures at $T = 50°C$, 60°C, and 70°C.

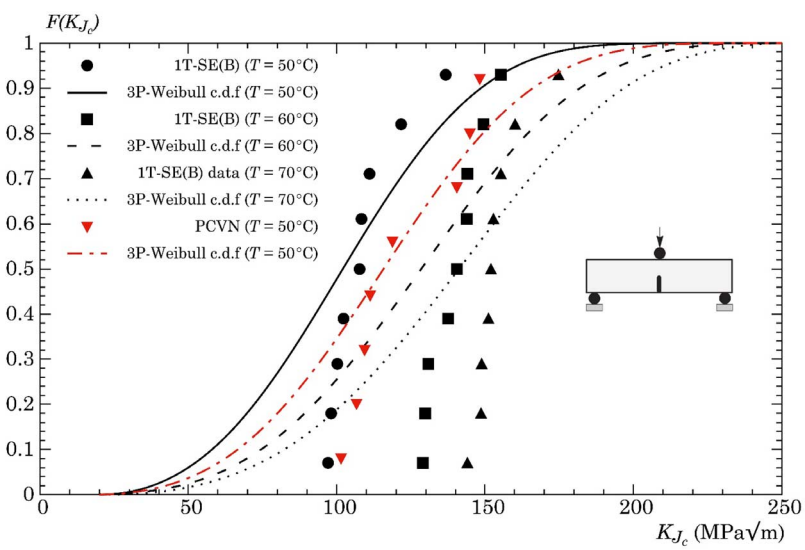

TABLE 4

Maximum likelihood estimates of the characteristic toughness, K_0, for the measured distributions of the K_{Jc}-values at varying test temperatures and the corresponding reference temperatures, T_0, evaluated from the single-temperature and multi-temperature methods

Geometry	T, °C	a	K_0, MPa$\sqrt{m}$	a	J_0, kJ/m²	$T_{0\text{-}ST}$, °C	$T_{0\text{-}MT}$, °C
1T SE(B)	50	4	112	6.9	115	47	
			(94, 134)		(104, 127)		
1T SE(B)	60	4	141	14.9	144	41	44
			(119, 167)		(138, 151)		
1T SE(B)	70	4	155	13.7	158	45	
			(130, 185)		(150, 167)		
PCVN	50	4	133	6.3	136	49	N/A
			(110, 162)		(121, 154)		

Note: N/A = not applicable.

experimental toughness values. The curves displayed in these plots describe the three-parameter Weibull distribution for K_{Jc}-values given by previous equation (2) with a fixed value $\alpha = 4$ to describe the scatter in test data as adopted by ASTM E1921-21a. **Table 3** shows the fracture toughness at cleavage instability for the martensitic steel tested at $T = 50$°C, 60°C, and 70°C, and also includes the average precrack fatigue length based on the nine-point measurement technique given by ASTM E1820-21. The table also provides the deformation limit, M, for each measured toughness data. **Table 4** provides the ML estimates of the characteristic toughness, $\hat{K}_0$, for all tested crack configurations derived from equation (5), including the 90 % confidence bounds given by Thoman[27] (see also Mann et al.[19]).

The key feature of these results is that there is a marked effect of temperature on fracture toughness as the characteristic toughness, K_0, increases rather distinctly with increased test temperature. Unfortunately, the experimental results are not particularly well-fit by equation (2) with a fixed value $\alpha = 4$. Although we have not investigated the source of such behavior, we argue that the predominantly martensitic microstructure associated with potential changes in the local cleavage micromechanism compared to conventional ferritic steels (see discussion in the review article of Hahn[28]) may be the cause of the reduced scatter in the experimental data —recall that the Weibull modulus characterizes the scatter in test data. However, as already noted by Ruggieri et al.,[29] ensuring a high fitting quality of the three-parameter Weibull distribution to the experimental data is not a requisite feature for strict applications of the MC procedure. To illustrate this issue, **Table 4** also provides both Weibull parameters, $\hat{\alpha}$ and $\hat{\beta}$, obtained from a standard ML estimation procedure and the corresponding 90 % confidence bounds for K_0.[19,27] Clearly, although large differences in parameter α are evidenced in these approaches, the sensitivity of the estimated K_0-value to the Weibull modulus is fairly small. For example, although the Weibull modulus changes from 4 to almost 15 in the case of the SE(B) specimen tested at $T = 60$°C, thereby characterizing a very small data scatter, differences in K_0-estimates are only ≈2 %. Therefore, we can conclude that even substantial changes in the Weibull modulus, which are associated with the degree of agreement between the Weibull distribution defined by equation (2) and the experimental data, result in only modest variations in parameter K_0 and, thus, have little effect on the T_0 evaluation for the martensitic steel addressed next.

Temperature Effects on Fracture Toughness

The following sections address the applicability of the MC approach to describe the effects of temperature on fracture toughness in terms of the reference temperature T_0 for the tested ultrahigh strength steel. The presentation begins with evaluation of T_0 based on the single temperature method at selected test temperatures. The analyses then proceed to determine the reference temperature using the multi-temperature approach.

SINGLE TEMPERATURE METHOD

Figures 7–9 describe the dependence of K_{Jc-med}, with temperature for three test temperatures: at $T = 50$°C, 60°C, and 70°C. In these plots, the solid lines define the MC of median toughness, K_{Jc-med}, whereas the dashed lines define the 5 % and 95 % tolerance bounds derived from ASTM E1921-21a procedure. The measured K_{Jc}-values at these test temperatures are also included in the plot to facilitate assessing the MC indexed by T_0 and, at the same time, how well the tolerance bounds envelop the measured fracture toughness data. Table 4 presents the corresponding single temperature T_0-values for each temperature, here denoted as T_{0-ST}.

Examination of these results reveals that, although there is no clear trend of a relationship between test temperature and the reference temperature, the estimated T_0 exhibits a relatively weak dependence over the range considered. This trend could be explained in terms of the somewhat small data set and the relatively poor fitting of the three-parameter Weibull distribution with $\alpha = 4$ to the experimental toughness values—refer to figure 6 and Table 4. A noteworthy additional feature of these results is that the estimated T_0-values and, thus, the test temperatures for the cases under consideration are much closer to T_{0-41J} for the tested material than T_{0-28J}—recall that the hyperbolic tangent curve fitting gave $\widetilde{T}_{0-28J} = -20.8$°C and $\widetilde{T}_{0-41J} = 66$°C. Although one would generally anticipate that T_{0-28J} provides good estimates of T_0 in the case of ferritic steels, the present results suggest that T_{0-41J} gives better estimates of the reference temperature for the ultrahigh strength steel under analysis.

Evaluation of the reference temperature for the data set tested at $T = 70$°C deserves further consideration. As briefly discussed in the section titled "Fracture Toughness Testing," the fracture surfaces of the specimens tested at this temperature displayed in figure 5*B* exhibited a predominantly dimple morphology, thereby suggesting that the local fracture is driven by a void growth mechanism rather than a stress-controlled cleavage. Nevertheless, the resulting reference temperature is $T_{0-ST} = 45$°C, which is, thus, in very close agreement with the T_0-value of 47°C for the data set tested at 50°C. This can be understood by the following argument. Whereas the MC methodology is conceptually applicable to stress-controlled cleavage fracture behavior of ferritic steels, thereby incorporating fracture toughness values under conditions sufficiently close to SSY, the procedure given by ASTM E1921-21a essentially relies on fitting K_{Jc}-values that satisfy specified deformation limits relative to specimen size to a three-parameter Weibull distribution. Even in the case of cleavage after small amounts of slow stable crack growth, ASTM E1921-21a does allow the use of a censoring model for the data set of K_{Jc}-values, regardless of the specific failure mode at fracture. The case under discussion falls exactly into this scenario as the deformation levels at

FIG. 7

Master curve for the tested martensitic steel, including 5 % and 95 % tolerance bounds, based on cleavage fracture toughness values measured from standard 1T SE(B) specimens tested at 50°C.

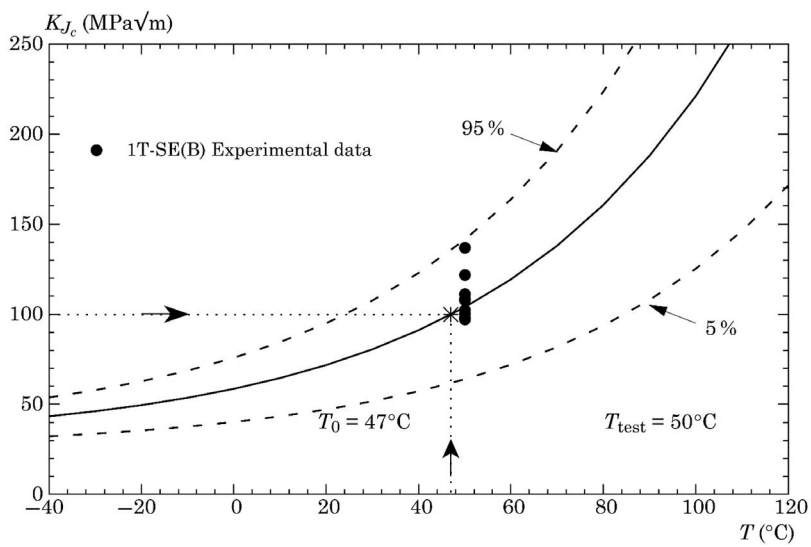

FIG. 8

Master curve for the tested martensitic steel, including 5 % and 95 % tolerance bounds, based on cleavage fracture toughness values measured from standard 1T SE(B) specimens tested at 60°C.

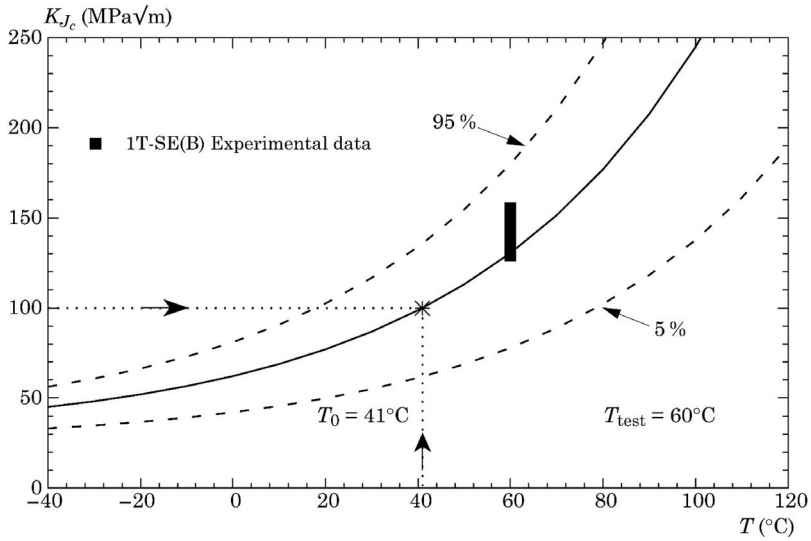

FIG. 9

Master curve for the tested martensitic steel, including 5 % and 95 % tolerance bounds, based on cleavage fracture toughness values measured from standard 1T SE(B) specimens tested at 70°C.

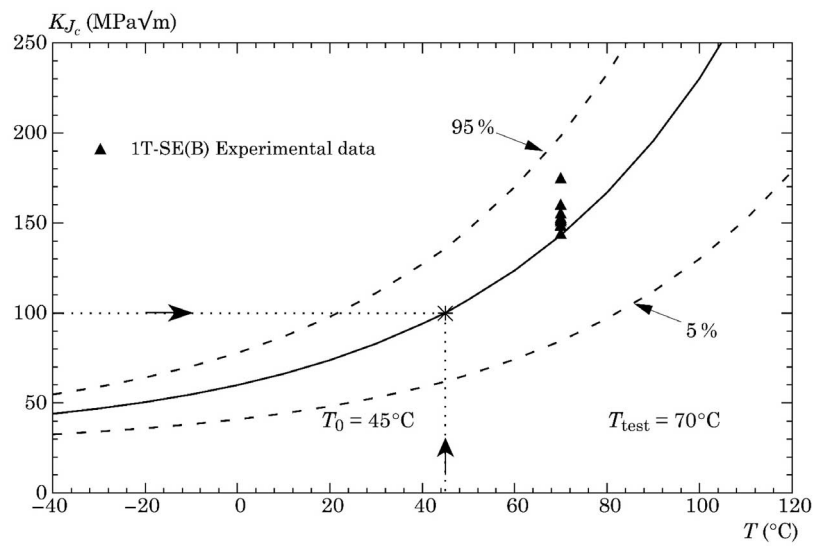

fracture characterized by the *M*-values for this data set are very high (refer to **Table 3**) and no ductile tearing prior to fracture instability is observed. Thus, even considering that no stress-controlled cleavage fracture occurred (which is one of the fundamental premises of the MC methodology) but, rather, fracture was predominantly controlled by a dimple mechanism at this temperature, we were able to obtain good estimates of the reference temperature in accordance with the MC methodology. As a consequence, there appears to be a strong indication that fitting the fracture toughness distribution with a 3P Weibull distribution is far more important than the specific micromechanics driving the fracture process. These arguments are also somewhat along the lines of the findings obtained in previous work of Odette et al.[8]. However, because this class of ultrahigh strength steel having a martensitic microstructure is currently beyond the reach of the MC methodology and ASTM E1921-21a,

FIG. 10

Master curve for the tested martensitic steel, including 5 % and 95 % tolerance bounds, based on cleavage fracture toughness values measured from subsize PCVN specimens tested at 50°C.

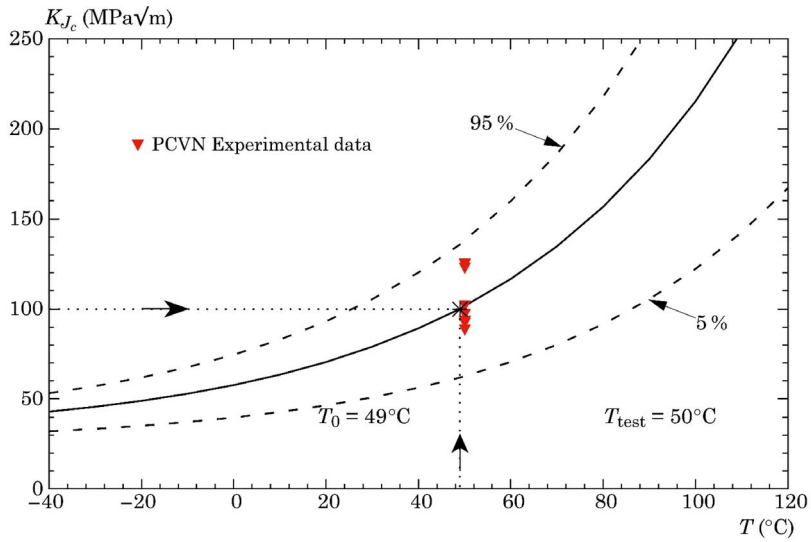

we avoid drawing definite conclusions but remain highly confident that the MC approach is effectively applicable to this case.

Application of the MC procedure to determine the reference temperature based on K_{Jc}-values measured from testing the subsize PCVN configuration is also of interest. Here, because the fracture specimens have a thickness of 10 mm, the corresponding toughness data must be first corrected to the equivalent 1T K_{Jc}-values using equation (4)—notice that the K_{Jc}-values shown in **Table 3** for this specimen configuration are the measured toughness data not the thickness corrected values. **Figure 10** displays the variation of K_{Jc-med}, with temperature derived from these fracture toughness data. **Table 4** also shows the corresponding T_{0-ST}. In this case, the estimated T_{0-ST} is slightly higher than the corresponding T_{0-ST}-value derived from testing the 1T SE(B) specimens at $T = 50$°C. Although both estimated T_0-values are still within an acceptable margin of difference, this particular result deserves further discussion. In previous work, Joyce and Tregoning[6] compare T_0-results derived from fracture toughness measurements obtained by testing both the PCVN configuration and larger specimen geometries, including C(T) and SE(B) specimens, for different pressure vessel steels. Their analyses show that Charpy size specimens generally provide lower T_0-values compared to the corresponding estimates from larger specimens, thereby yielding slightly nonconservative evaluations of the reference temperature. Similar findings were also reported by Sokolov and Nanstad[30] as well as in ASTM E1921-21a. However, Joyce and Tregoning[6] attributed the cause of these trends to the level of constraint at fracture in connection with the relatively small sampling size and material variability at crack front for small size specimens. For the PCVN configuration under consideration, the levels of specimen deformation described by the M-values are consistently high, with several specimens exhibiting $M \geq 100$, which suggests that the present data set is essentially not affected by constraint loss. Whether analogous results occur in other classes of high strength steels with predominantly martensitic microstructure is currently unknown and we consider this issue an open question.

MULTI-TEMPERATURE METHOD

Although the method based on a single test temperature described previously provides a straightforward procedure to determine T_0 with adequate reliability, application of the multi-temperature method defined by equation (9) gives additional insight into the effectiveness of the MC methodology to evaluate the reference temperature for the tested martensitic steel. Within the present context, such may be justified by considering

FIG. 11

Master curve for the tested martensitic steel, including 5 % and 95 % tolerance bounds, based on the multi-temperature method using cleavage fracture toughness values measured from standard 1T SE(B) specimens tested at 50°C, 60°C and 70°C.

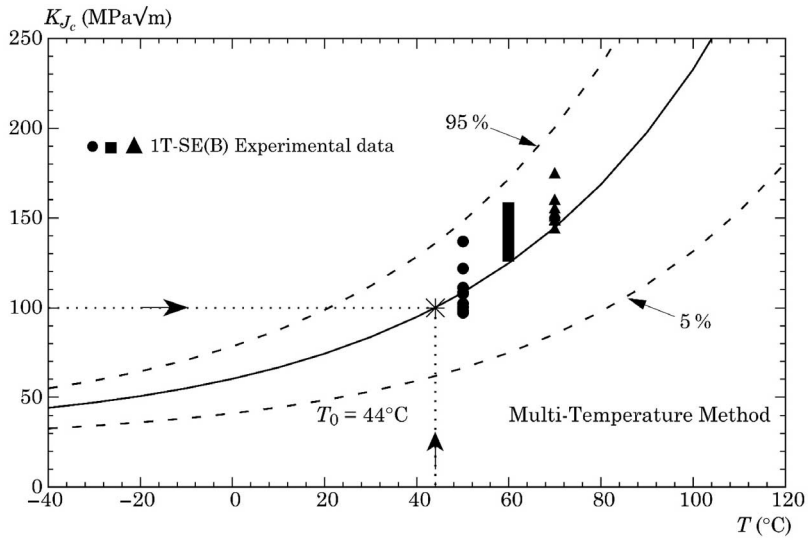

that the single temperature approach is a special case of the multi-temperature procedure, so that the latter method should presumably yield the most accurate T_0 estimate.

Figure 11 shows the MC and associated confidence bounds based on the multi-temperature method using cleavage fracture toughness values measured from standard 1T SE(B) specimens tested at $T = 50$°C, 60°C, and 70°C. Table 4 provides the corresponding T_0-value, here denoted as T_{0-MT}. This analysis is rather conclusive. The reference temperature evaluated by the multi-temperature method result in a T_0 estimate that is in close agreement with other single temperature estimates. Observe, however, when taking T_{0-MT} as the "correct" reference temperature, it can be seen that the estimated T_{0-ST}-values at $T = 50$°C and 70°C are slightly larger, whereas the estimated T_{0-ST}-value at $T = 60$°C is nonconservatively biased. Thus, although we would again hesitate to draw definite conclusions, these results suggest that evaluation of the reference temperature using solely the multi-temperature method would likely be the best choice in the present case.

Concluding Remarks

This study describes an application of the MC methodology, originally developed for ferritic steels, to determine the indexed reference temperature, T_0, for an ultrahigh strength steel with predominantly martensitic microstructure. The analyses comprise both the single-temperature and the multi-temperature methods. A primary objective of the present work is to assess the effectiveness of the procedure to provide reliable estimates of T_0 derived from fracture toughness data sets measured from testing standard 1T SE(B) specimens at different temperatures over the DBT region for this class of material. As a second objective, the investigation also evaluates the reference temperature for the tested steel using PCVN configurations. The analyses described in this work supports the following conclusions:

- Evaluation of the reference temperature, T_0, appears to be mainly controlled by the statistically-based model to describe fracture toughness values, K_{Jc}, under high constraint conditions rather than details of the specific failure mode associated with the steel microstructure.
- Ensuring a high fitting quality of the three-parameter Weibull distribution to the experimental data is not a requisite feature for strict applications of the MC procedure, as the scale parameter, K_0, of the 3P Weibull distribution describing the K_{Jc}-values is not very sensitive to large changes in parameter α.

- The indexing temperature, $\widetilde{T}0$, which serves as the basis for the test temperature, is more accurately estimated from the Charpy transition temperatures corresponding to 41 J, T_{41J}, for the tested ultrahigh strength, martensitic steel.
- Evaluation of the reference temperature based on the multi-temperature method appears to provide more reliable estimates of T_0 for the tested material and, thus, would likely be the best choice in routine applications of the MC procedure.

Although the ultrahigh strength, martensitic steel employed in the present work does not fall into the category of ferritic steels encompassed by the MC methodology and ASTM E1921-21a, the procedure still appears to provide accurate estimates of the reference temperature and, thus, a good description of the fracture toughness dependence with temperature for the tested material. A reason offered for this outcome is that fitting a three-parameter Weibull distribution to K_{Jc}-values that satisfy specified deformation limits relative to specimen size is viewed as effectively offsetting any potential effects of the specific failure mode at the microlevel. Although these conclusions are born out in the results that are obtained from limited experimental data sets, the fact that the estimated T_0-values appear mostly consistent with the expected trends lends hope that further progress may be made in effectively extending the MC methodology to this class of high strength steels. Specifically, more extensive data sets covering a wider range of UHSS obtained by different production routes and having varying microalloying are needed.

ACKNOWLEDGMENTS

This investigation is supported by Fundação de Amparo à Pesquisa do Estado de São Paulo (FAPESP) through research grant 2020/01903-8. The second author (V.M.C.G.) would like to acknowledge the financial support from Coordenação de Aperfeiçoamento de Pessoal de Nível Superior (CAPES). The work of the third author (C.R.) is also supported by the Brazilian Council for Scientific and Technological Development (CNPq) through grant 302853/2018-9.

References

1. K. Wallin, "Fracture Toughness Transition Curve Shape for Ferritic Structural Steels," in *Fracture of Engineering Materials and Structures*, ed. S. H. Teoh and K. H. Lee (Dordrecht, the Netherlands: Springer, 1991), 83–88.
2. K. Wallin, "Irradiation Damage Effects on the Fracture Toughness Transition Curve Shape for Reactor Pressure Vessel Steels," *International Journal of Pressure Vessels and Piping* 55, no. 1 (1993): 61–79, https://doi.org/10.1016/0308-0161(93)90047-W
3. K. Wallin, "Master Curve Analysis of the Euro Fracture Toughness Dataset," *Engineering Fracture Mechanics* 69, no. 4 (March 2002): 451–481, https://doi.org/10.1016/S0013-7944(01)00071-6
4. J. G. Merkle, K. Wallin, and D. E. McCabe, "Technical Basis for an ASTM Standard on Determining the Reference Temperature, T_0, for Ferritic Steels in the Transition Range," in *Oak Ridge National Laboratory, Technical Report No. ORNL/TM-13631* (Washington, DC: US Nuclear Regulatory Commission, 1998).
5. D. E. McCabe, J. G. Merkle, and K. Wallin, *An Introduction to the Development and Use of the Master Curve Method*, (Conshohocken, PA: ASTM International, 2005), https://doi.org/10.1520/MNL52-EB
6. J. A. Joyce and R. L. Tregoning, "Development of the T_0 Reference Temperature from Precracked Charpy Specimens," *Engineering Fracture Mechanics* 68, no. 7 (May 2001): 861–894, https://doi.org/10.1016/S0013-7944(00)00135-1
7. American Society of Mechanical Engineers, *Boiler and Pressure Vessel Code, ASME BPVC-21* (New York: American Society of Mechanical Engineers, 2021).
8. G. R. Odette, T. Yamamoto, H. Kishimoto, M. Sokolov, P. Spätig, W. J. Yang, J. W. Rensman, and G. E. Lucas, "A Master Curve Analysis of F82H Using Statistical and Constraint Loss Size Adjustment of Small Specimen Data," *Journal of Nuclear Materials* 329–333, Part B (August 2004): 1243–1247, https://doi.org/10.1016/j.jnucmat.2004.04.255
9. P. Mueller, P. Spätig, R. Bonadé, G. R. Odette, and D. Gragg, "Fracture Toughness Master-Curve Analysis of the Tempered Martensitic Steel Eurofer97," *Journal of Nuclear Materials* 386–388 (April 2009): 323–327, https://doi.org/10.1016/j.jnucmat.2008.12.122
10. A. Neimitz, I. Dzioba, and T. Limnell, "Modified Master Curve of Ultra High Strength Steel," *International Journal of Pressure Vessels and Piping* 92 (April 2012): 19–26, https://doi.org/10.1016/j.ijpvp.2012.01.008
11. A. Neimitz, I. Dzioba, and T. Pala, "Master Curve of High-Strength Ferritic Steel S960-QC," *Key Engineering Materials* 598 (January 2014): 178–183, https://doi.org/10.4028/www.scientific.net/KEM.598.178

12. K. Wallin, S. Pallaspuro, I. Valkonen, and P. Karjalainen-Roikonen, "Fracture Properties of High-Performance Steels and Their Welds," *Engineering Fracture Mechanics* 135 (February 2015): 219–231, https://doi.org/10.1016/j.engfracmech.2015.01.007
13. N. Baluc, R. Schäublin, P. Spätig, and M. Victoria, "On the Potentiality of Using Ferritic/Martensitic Steels and Structural Materials for Fusion Reactors," *Nuclear Fusion* 44, no. 7 (December 2003): 56–61, https://doi.org/10.1088/0029-5515/44/1/006
14. International Atomic Energy Agency, *Guidelines for Application of the Master Curve Approach to Reactor Pressure Vessel Integrity in Nuclear Power Plants, Technical Report 429* (Vienna, Austria: International Atomic Energy Agency, 2005).
15. S. Yukawa and J. Merkle, "Development of the Present Reference Fracture Toughness Curves in the ASME Nuclear Code" (paper presentation, Proceedings of the ASME 1984 Pressure Vessels and Piping Conference, San Antonio, TX, 1984).
16. H. W. Viehrig, J. Boehmert, and J. Dzugan, "Some Issues by Using the Master Curve Concept," *Nuclear Engineering and Design* 212, nos. 1–3 (March 2002): 115–124, https://doi.org/10.1016/S0029-5493(01)00465-4
17. T. L. Anderson, *Fracture Mechanics: Fundaments and Applications*, 4th ed. (Boca Raton, FL: CRC Press, 2017).
18. K. Wallin, "The Scatter in K_{Ic} Results," *Engineering Fracture Mechanics* 19, no. 6 (1984): 1085–1093, https://doi.org/10.1016/0013-7944(84)90153-X
19. N. R. Mann, R. E. Schafer, and N. D. Singpurwalla, *Methods for Statistical Analysis of Reliability and Life Data* (New York: John Wiley & Sons, 1974).
20. H. Rinne, *The Weibull Distribution: A Handbook*, 1st ed. (New York: Chapman and Hall/CRC, 2008).
21. K. Wallin, "Validity of Small Specimen Fracture Toughness Estimates Neglecting Constraint Corrections," in *Constraint Effects in Fracture: Theory and Application*, ed. M. Kirk and A. Bakker (Conshohocken, PA: ASTM International, 1995), 519–537, https://doi.org/10.1520/STP14650S
22. F. C. Campbell, "Nonequilibrium Reactions: Martensitic and Bainitic Structures," in *Phase Diagrams: Understanding the Basics* (Materials Park, OH: ASM International, 2012), 303–338.
23. American Petroleum Institute, *Fitness-for-Service, API RP-579-1/ASME FFS-1* (Washington, DC: American Petroleum Institute, 2021).
24. W. Oldfield, "Fitting Curves to Toughness Data," *Journal of Testing and Evaluation* 7, no. 6 (November 1979): 326–333, https://doi.org/10.1520/JTE11508J
25. M. T. Erickson Kirk, A. Shaikh, and M. A. Erickson Kirk, "Insights and Observations Arising from Curve-Fitting the Charpy V-Notch and Tensile Data Contained Within the United States Light Water Reactor Surveillance Database," in *Proceedings of the ASME 2008 Pressure Vessels and Piping Conference, Volume 3: Design and Analysis* (New York: American Society of Mechanical Engineers, 2008), 389–396.
26. J. H. Chen and R. Cao, *Micromechanism of Cleavage Fracture of Metals: A Comprehensive Microphysical Model for Cleavage Cracking in Metals*, 1st ed. (Oxford, UK: Butterworth-Heinemann, 2014).
27. D. R. Thoman, L. J. Bain, and C. E. Antle, "Inferences on the Parameters of the Weibull Distribution," *Technometrics* 11, no. 3 (August 1969): 445–460.
28. G. T. Hahn, "The Influence of Microstructure on Brittle Fracture Toughness," *Metallurgical Transactions A* 15, no. 6 (June 1984): 947–959, https://doi.org/10.1007/BF02644685
29. C. Ruggieri, R. G. Savioli, and R. H. Dodds, "An Engineering Methodology for Constraint Corrections of Elastic-Plastic Fracture Toughness—Part II: Effects of Specimen Geometry and Plastic Strain on Cleavage Fracture Predictions," *Engineering Fracture Mechanics* 146 (September 2015): 185–209, https://doi.org/10.1016/j.engfracmech.2015.06.087
30. M. Sokolov and R. Nanstad, "On Bias in T_0 Values Derived with Compact and PCVN Specimens," in *Proceedings of the ASME/JSME 2004 Pressure Vessels and Piping Conference. Fracture Methodologies and Manufacturing Processes* (New York: American Society of Mechanical Engineers, 2004), 115–120.